NASA TECHNICAL MEMORANDUM

NASA TM X-3367

NASA TM X-3367

AERODYNAMIC PERFORMANCE OF FLARED FAN NOZZLES USED AS INLETS

Donald A. Dietrich, Theo G. Keith, and Gary G. Kelm

Lewis Research Center
Cleveland, Ohio 44135

NATIONAL AERONAUTICS AND SPACE ADMINISTRATION • WASHINGTON, D. C. • MARCH 1976

1. Report No.	2. Government Accession No.	3. Recipient's Catalog No.
NASA TM X-3367		

4. Title and Subtitle	5. Report Date
AERODYNAMIC PERFORMANCE OF FLARED FAN NOZZLES USED AS INLETS	March 1976
	6. Performing Organization Code
7. Author(s)	8. Performing Organization Report No.
Donald A. Dietrich, Theo G. Keith, and Gary G. Kelm	E-8539
	10. Work Unit No.
9. Performing Organization Name and Address	505-05
Lewis Research Center National Aeronautics and Space Administration Cleveland, Ohio 44135	11. Contract or Grant No.
	13. Type of Report and Period Covered
12. Sponsoring Agency Name and Address	Technical Memorandum
National Aeronautics and Space Administration Washington, D. C. 20546	14. Sponsoring Agency Code

15. Supplementary Notes

16. Abstract

Tests were conducted in a low-speed wind tunnel to determine the aerodynamic performance of several flared fan nozzles. Each of the flared nozzles was a downstream-facing inlet to a model fan that was used to simulate a variable-pitch fan during reverse-thrust operation. The total pressure recovery of each of the flared nozzles as well as that of an unflared nozzle and a serrated-flare nozzle was obtained for comparison. The aerodynamic performance of a selected flared nozzle was considered in further detail. The nozzle surface pressures for a flared nozzle were also determined. Results indicated that the differences in aerodynamic performance among the nozzles were most apparent at the wind-tunnel-off condition. A nonzero free-stream velocity significantly reduced the performance of all the nozzles, and crosswind flow (free-stream flow perpendicular to the model axis) further reduced the performance of the nozzles. The unflared nozzle and the serrated-flare nozzle had reduced aerodynamic performance compared to a solid-surface flared nozzle.

17. Key Words (Suggested by Author(s))

Thrust reversing
Propulsion systems
Model testing
Wind tunnel testing
Inlet
Nozzle

18. Distribution Statement

Unclassified - unlimited
STAR Category 07 (rev.)

19. Security Classif. (of this report)	20. Security Classif. (of this page)	21. No. of Pages	22. Price*
Unclassified	Unclassified	30	$3.75

* For sale by the National Technical Information Service, Springfield, Virginia 22161

AERODYNAMIC PERFORMANCE OF FLARED FAN NOZZLES USED AS INLETS

by Donald A. Dietrich, Theo G. Keith,* and Gary G. Kelm

Lewis Research Center

SUMMARY

Tests were conducted in a low-speed wind tunnel to determine the aerodynamic performance of several flared fan nozzles. Each of the flared nozzles was a downstream-facing inlet to a model fan that was used to simulate a variable-pitch fan during reverse-thrust operation. The total pressure recovery of each of the flared nozzles as well as that of an unflared nozzle and a serrated-flare nozzle was obtained for comparison. The aerodynamic performance of a selected flared nozzle was considered in further detail. The nozzle surface pressures for a flared nozzle were also determined. Results indicated that the differences in aerodynamic performance among the nozzles were most apparent at the wind-tunnel-off condition. A nonzero free-stream velocity significantly reduced the performance of all the nozzles, and crosswind flow (free-stream flow perpendicular to the model axis) further reduced the performance of the nozzles. The unflared nozzle and the serrated-flare nozzle had reduced aerodynamic performance compared to a solid-surface flared nozzle.

INTRODUCTION

In recent years there has been considerable study of the suitability of a variable-pitch fan engine for short-haul aircraft applications. References 1 to 5 discuss the advantages of a variable-pitch fan and indicate that the fan pitch may be varied to achieve both forward-thrust modulation and reverse thrust. The experiment reported herein was conducted to investigate the aerodynamic performance of fan nozzle configurations during thrust reversal.

Figure 1 illustrates the elements of a variable-pitch fan engine during reverse-thrust operation. The chord angles of the fan blades are oriented such that flow is drawn into the fan duct through the fan nozzle, which may be flared (as shown in fig. 1)

*Assistant Professor of Mechanical Engineering, University of Toledo, Toledo, Ohio; Summer Faculty Fellow at the Lewis Research Center in 1973 and 1974.

to improve aerodynamic performance. The fan flow is then exhausted through the inlet in the direction counter to the direction of the free-stream flow. Thus, in reverse thrust the fan nozzle acts as an inlet and the fan inlet acts as a nozzle. The combination of the words exit (nozzle) and inlet into the term "exlet" is used throughout this report to refer to the fan nozzle when it is being used as an inlet with variable-pitch reverse flow.

Variable-pitch fans operate with a small total pressure rise across the fan. Thus, any loss in total pressure recovery in the exlet severely reduces the available reverse thrust. Furthermore, it may be desired that the fan operate at a low noise level during thrust reversal. But an increase in the engine power setting to compensate for the losses in the exlet may increase the noise level. The level of the fan flow (intake) distortion is also significant because a distorted intake flow may reduce stall margin, increase fan noise, and increase blade vibrational stress. In addition, the core inlet and core exhaust flows must be sufficiently similar to forward-thrust operation that the core engine operation is not adversely affected.

Little information exists on the performance of an exlet. Reference 6 presents a method of analyzing the aerodynamic performance (in terms of total pressure recovery) of a sharp-lip forward thrust (or unflared) nozzle used as an exlet. That analysis shows that the exlet total pressure recovery is always less than free-stream static pressure. Reference 7 is an experimental report similar to this report, but the data were obtained from a model of somewhat different geometry.

The primary consideration of this report is the aerodynamic performance of several flared exlets. However, some consideration is also given to the interaction of fan exhaust flow and free-stream flow, to the effect of the exlet performance on the quality of the flow available to the core inlet, and to the exlet surface static pressures. Experimental results are presented on the aerodynamic performance at static and forward velocity conditions of a series of exlet geometries encompassing several flare lengths, flare angles from 0° to 60°, and a serrated-flare exlet. The aerodynamic performance is presented in terms of the total pressure recovery, total pressure distributions, and fan flow distortion parameters. The program was conducted in a low-speed wind tunnel at free-stream Mach numbers from 0 to 0.21 and crosswind (flow perpendicular to the fan axis) velocities from 0 to 20 meters per second. Tests were conducted at fan-intake-duct Mach numbers from 0.20 to 0.55.

SYMBOLS

A point of junction between internal flare (exlet) and fan duct

B exlet tip

CR exlet contraction ratio (i. e., ratio of annular area at exlet tip to annular fan duct area), $CR = \left(d_e^2 - d_h^2\right)/\left(d_f^2 - d_h^2\right)$

D fan duct flow distortion parameter, (Maximum total pressure - Minimum total pressure)/(Area-averaged total pressure)

d_e model diameter at exlet tip, cm

d_f outer diameter in fan duct, 13. 97 cm

d_h centerbody diameter in fan duct, 5. 08 cm

h passage height in fan duct, 4. 45 cm

L distance from rake measuring plane to flare/fan-duct junction (point A), 10. 16 - l_e, cm

l_e exlet length measured along internal flow surface between points A and B, cm

M_a component of free-stream Mach number along model centerline

M_0 free-stream Mach number

M_1 Mach number in fan duct at rake measuring plane

N fan rotational speed, rpm

N_d design fan rotational speed, 35 800 rpm

P total pressure, N/m^2

P_{le} average total pressure of outermost three tubes on each rake at rake measuring plane, N/m^2

P_{li} average total pressure of innermost three tubes on each rake at rake measuring plane, N/m^2

P_r average total pressure of innermost ring of tubes at rake measuring plane, N/m^2

p static pressure, N/m^2

p_f static pressure measured on exlet surface, N/m^2

V_c component of free-stream velocity perpendicular to model axis, m/sec

θ_e exlet flare angle (i. e., angle between internal flare surface and model centerline), deg

Subscripts:

0 free-stream station

1 rake measuring plane station

APPARATUS AND PROCEDURE

Fan/Nacelle Model

Figure 2 is a sketch of the fan/nacelle model with a representative exlet. The model was arranged in such a manner that flow was drawn into the fan through the exlet and exhausted in a direction counter to that of the free-stream flow. In the model a commercially available fan was used only as a flow generator and not as a model of an actual variable-pitch fan. The entire fan/nacelle model was mounted from a swept, vertically oriented pylon and consisted of an inlet section, a reversed-fan section, a fan duct section, and an exlet section. Each of these sections is discussed in detail here.

Exlet design. - The basic features of each of the exlets tested are shown in figure 3. The exlet is mounted on the model at the rake measuring plane (fig. 3(a)). Each exlet includes the same fan duct centerbody, which protrudes beyond the end of the exlet to simulate the core engine (fig. 1) and has a constant diameter throughout the exlet section.

The internal surface of each exlet is a composite of annular and conic surfaces, as shown in figure 3. Immediately past the rake measuring plane (with respect to the fan flow), the internal flow passage is annular. The outside diameter is 13.97 centimeters and the inside diameter is 5.08 centimeters. At point A, the internal flow passage becomes conical, and the conical half-angle of that surface is called the exlet flare angle θ_e. Point B is the exlet tip or highlight, and the distance from point A to point B is the exlet flare length l_e. The exlet test configurations are made up of various combinations of exlet flare angle and flare length. However, all of the exlets have the same total distance of 10.16 centimeters measured along the internal surface from point B to the rake measuring plane and have machined radii of 0.05 centimeter at points A and B.

The external surface of each exlet is composed of cylindrical and conical surfaces. The maximum nacelle diameter, excluding the exlet flare, is 16.5 centimeters. A break in the external surface occurs 1.78 centimeters downstream (with respect to the free-stream flow) from the rake measuring plane. At this point, a 9° nozzle boattail angle is used. The angle between the internal and external exlet surfaces is also 9° for all exlet flare configurations.

Fan. - The fan used in these tests has a fixed rotor-blade pitch angle rather than variable pitch. Thus, the fan is mounted (fig. 2) opposite to the common orientation with respect to the direction of the free-stream flow to simulate a variable-pitch fan during thrust reversal. The fan rotor has a tip diameter of 13.97 centimeters and, at the design rotational speed of 35 800 rpm, passes a mass flow of 2.49 kilograms per second at a pressure ratio of 1.25. The fan is driven by a tip turbine (fig. 2) that, at the fan design speed, required a mass flow of 0.47 kilogram per second of unheated air at a turbine-plenum pressure of 2590 kN/m^2. Further information on the basic fan is

reported in reference 8.

Inlet. - A representative (forward-thrust case) inlet is used for all tests. The inlet (fig. 2) has a total length from stator exit to inlet highlight of 13.7 centimeters, a maximum diameter of 16.5 centimeters, and a throat diameter of 14.0 centimeters. The diffuser portion of the inlet is basically conical in shape with some contouring in the regions of the stator exit and the inlet lip. The inlet lip is elliptic and has an inlet contraction ratio (highlight- to throat-area ratio) of 1.29. Also included in the inlet section is a centerbody representative of that used on a variable-pitch-fan inlet.

Instrumentation. - The instrumentation used during the test program is illustrated in figure 3. The primary elements of the instrumentation are the total pressure rakes and associated wall static pressure taps located at the rake measuring plane. The total pressure rakes are located 10.16 centimeters downstream (with respect to the fan flow) from the exlet highlight (point B) for all the exlets. Therefore, the rake measuring plane is located a different distance, L, from point A for each exlet, that is, $L = 10.16 - l_e$ (fig. 3(a)). As shown in figure 3(b), eight radial total pressure rakes are spaced 45° apart, with the first rake located at the 0° position (directly opposite the pylon). The convention used for the circumferential angle is shown in figure 3(b). Each rake has six equal-area-weighted total pressure tubes (fig. 3(a)). Seven static pressure taps are located on the outer wall of the flow passage midway between the total pressure rakes (fig. 3(b)).

The total and static pressure measurements are used to determine both the total pressure recovery and the fan duct Mach number, which are determined in the same manner as in reference 9. The total pressure recovery is the ratio of the area-averaged rake measurements at the rake measuring plane (fig. 3(a)) and the free-stream total pressure. The fan duct Mach number is the value calculated from the measured mass flow, which in turn is determined from the total pressure, the duct area, and the static pressure. Calculations of the fan duct Mach number are based on an assumed constant static pressure across the duct, which is substantiated by the data of reference 7.

Exlet flare instrumentation was installed on only one of the exlets. The axial location of the instrumentation is shown in figure 3(c). That instrumentation consisted of the following: four internal-flow-passage static pressure taps at each of four circumferential locations (0°, 90°, 180°, and 270°), four external-flow-passage static pressure taps at each of two circumferential locations (100° and 280°), and two external-flow-passage total pressure tubes (opposite facing tubes shown in fig. 3(c)) at each of two circumferential locations (95° and 275°). The static pressure instrumentation was used to determine the exlet flare surface pressures, and the total pressure measurements were used only to determine the direction of the free-stream flow along the external flare surface.

Test Configurations

The first seven columns of table I contain the necessary information to describe the geometry of each of the nine exlets tested. The second column gives an abbreviated identification for each of the exlets that will be used throughout the written portion of this report. The third column associates a specific symbol shape with each exlet that will be used on the graphical presentation of the data. The fourth column contains small, schematic sketches of the exlets, with the location of the rake measuring plane indicated by the dashed line. Columns five to seven present the flare angle θ_e, the flare contraction ratio CR, and the flare length ratio l_e/h. The flare angle θ_e ranges from 30^o to 60^o, plus the limiting case of $\theta_e = 0^o$. The flare contraction ratio is the ratio of the annular areas at the exlet tip (point B, fig. 3(a)) and the rake measuring plane. The contraction ratio varies from 1.51 to 2.74, again plus the limiting case of 1.00. The flare length ratio is the ratio of the flare length l_e to the fan duct height h. The range of values of the flare length ratio is from 0.45 to 1.30.

The last two exlets shown in table I are special cases. The $\theta_e = 0^o$ (CR = 1.0) flare exlet represents an unflared or unopened nozzle that corresponds to a representative forward-thrust nozzle. The last configuration is a serrated-flare exlet (fig. 3(d)). This exlet was constructed by removing portions of the nominal 45^o-flare exlet (configuration 1) so that the remaining material represents 15 leaves of an expanding forward-thrust nozzle. Detailed information about the serrated exlet is contained in figure 3(d).

The first eight configurations listed in table I comprise the group of solid-flare exlets. The location of each of these eight exlets within a configuration-geometry matrix is shown in figure 4, in which exlet contraction ratio is a function of exlet flare angle. The solid lines denote constant flare length ratio l_e/h. As figure 4 shows, the nominal 45^o-flare exlet (circular symbol) acts as the central configuration for the geometry matrix. This exlet, the short 60^o-flare exlet, and the long 30^o-flare exlet as a group all have the same contraction ratio (CR = 2.1), as indicated by the vertical dashed line. Similarly, figure 4 (horizontal dashed line) and table I show there are three exlets having the same flare angle ($\theta_e = 45^o$) and three exlets having the same flare length ($l_e/h = 0.89$).

Test Facility

The test program was conducted in the Lewis Research Center's 9- by 15-Foot V/STOL Wind Tunnel, which is described in reference 10. The fan/exlet model installed in the test section is shown in figure 5. The vertically oriented pylon was attached to a horizontal model support post. This placed the model centerline 1.37 meters above the floor, 2.59 meters from one of the side walls, and 1.98 meters from the other side wall

under zero crosswind conditions ($V_c = 0$). To obtain nonzero crosswind conditions, the support post, pylon, and model were rotated above a vertical axis located 1.2 meters to the right of the model centerline as viewed in figure 5.

Test Procedure

The same procedure was followed during all tests. The free-stream velocity was set with the model axis alined with the free-stream flow. The fan was then operated at 40, 55, 70, 85, and 100 percent of the design rotational speed for the purpose of taking data. Without changing the free-stream velocity, the model was rotated to obtain a specified crosswind flow velocity (component of free-stream velocity perpendicular to model centerline). Then data were again taken at the same rotational speeds listed previously. This procedure deviates from the procedure used in similar tests on fan inlets (ref. 9). However, this procedure is more representative of the conditions encountered by a variable-pitch fan in operation. During each test condition, multiple readings were made and the data were averaged to obtain the results presented in this report.

Unflared Exlet

A variable-pitch fan engine has a nozzle that is unflared (or slightly convergent) for use during forward-thrust operation. Knowledge of the aerodynamic performance of a representative forward-thrust nozzle or an unflared exlet is important for two reasons. First, if the aerodynamic performance of the unflared exlet were sufficiently high, an additional mechanism to flare the nozzle would be unnecessary. Second, this information is required to analyze the resulting reverse thrust if during the thrust- or flow-reversing operation the mechanism failed to flare the nozzle.

Figure 6 presents both the total pressure recovery P_1/P_0 and the fan duct (measuring plane) Mach number M_1 as a function of free-stream Mach number M_0 for several percentages of design speed N/N_d for the 0^o-flare (unflared) exlet. It is readily apparent from figure 6(a) that the total pressure recovery of the unflared exlet is very low at the higher N/N_d (e.g., $P_1/P_0 \leq 0.92$ for $N/N_d \geq 85$ percent). Also shown for reference (dashed curve in fig. 6(a)) is the ratio of free-stream static to free-stream total pressure. The unflared exlet total pressure is always less than free-stream static pressure, which is a result consistent with the analysis of reference 6. A representative operating range for the fan duct Mach number of 0.4 to 0.5 has been chosen based on reference 7. Therefore, the values of total pressure recovery in table I are for a fan duct Mach number of 0.46, which approximates a test condition for every exlet. However, the pressure recovery listed in table I for the unflared exlet is an estimated

value (obtained by extrapolation of the data) since a fan duct Mach number of 0.46 could not be achieved for this configuration, as indicated in figure 6(b).

The low values of the fan duct Mach number are due primarily to the low total pressure recovery, which in general drops as the free-stream Mach number is increased. For high percentages of design speed (e.g., N/N_d = 100 percent), the fan duct Mach number drops from around 0.40 at $M_0 = 0$ to 0.35 at $M_0 = 0.21$. This drop in Mach number is due to the loss in exlet total pressure alone. It is not attributable to an interaction between the free-stream and fan exhaust flows, which could act to backpressure the fan and change the fan operating point. However, for low percentages of design speed (e.g., N/N_d = 40 percent), the mass flow drops sharply at high free-stream Mach numbers. For this exlet, flow could not be passed through the fan when N/N_d = 40 percent and $M_0 = 0.21$. Therefore, for some free-stream Mach number there is a lower limit on rotational speed (or rotor total pressure rise) below which the fan cannot pass flow and is stalled. In the region where the fan duct Mach number decreases sharply and approaches zero, the total pressure recovery approaches the ratio of free-stream static pressure to free-stream total pressure (dashed curve in fig. 6(a)). This result is predicted in reference 6. The results (low pressure recovery and low fan duct Mach number) of figure 6 demonstrate that the variable-pitch fan cannot be efficiently operated during reversing with the use of the forward-thrust (unflared) fan nozzle. Thus, a flared exlet can be considered as one possible way to improve the efficiency of operation.

Solid-Flare Exlets

The aerodynamic performance of all the solid-flare exlets is compared on the basis of total pressure recovery. A principal purpose of this comparison is to select the best exlet of those tested for use in a more detailed study of its performance.

Performance variation with fan duct Mach number. - Figures 7 to 9 present the total pressure recovery P_1/P_0 for all the solid-flare exlets (including some of the 0°-flare exlet data) as a function of fan duct Mach number. The symbols in this figure (and all other figures) correspond to specific configurations in table I. Each figure presents data for a specific subgroup of the exlet geometry matrix previously indicated in figure 4. Figure 7 contains data for all the exlets having the same flare length ($l_e/h = 0.89$); figures 8 and 9 present data for the exlets having the same contraction ratio (CR = 2.10) and the same flare angle ($\theta_e = 45^\circ$), respectively. Parts a, b, and c of these figures present data for constant values of the free-stream Mach number M_0 of 0, 0.13, and 0.21. The crossflow velocity V_c is zero for each case.

Figures 7 to 9 illustrate that the largest variation in pressure recovery with both fan duct Mach number and all geometric variables occurs at the static free-stream con-

dition, $M_0 = 0$ (figure parts (a)). For reference, the total pressure recovery at $M_0 = 0$ and $M_1 = 0.46$ is given for each configuration in the last column of table I. For these conditions, the total pressure recovery varied from 0.996 for the long 30°-flare exlet to 0.969 for the long 60°-flare exlet. At the static free-stream condition, the 30°-flare exlets have the highest total pressure recovery and the 60°-flare exlets have the lowest total pressure recovery of the flared exlets over the entire range of fan duct Mach numbers. The total pressure recovery of the 0°-flare exlet (figs. 6 to 9 and table I) is much lower than that of the flared configuration as previously noted.

The effect of free-stream velocity on the total pressure recovery may be seen by comparing the various parts of each of figures 7, 8, and 9. Increasing the free-stream Mach number significantly reduces the total pressure recovery of all the exlets. However, at a nonzero free-stream velocity the spread in pressure recovery due to fan duct Mach number or geometric parameters is much less than that at the static free-stream condition, excluding the short 45°-flare exlet. The one configuration that shows noticeably lower pressure recovery than all the other exlets (figs. 9(b) and (c)) is the short 45°-flare exlet. It also has the lowest contraction ratio (CR = 1.51). Therefore, based on the data of this report, the pressure recovery of all the exlets at forward velocity can be taken to be approximately the same value provided the contraction ratio is higher than about 1.74.

In general, figures 7 to 9 show that the total pressure recovery of the exlets is rather high considering the unusual flow patterns. This is true even at the free-stream Mach number of 0.21, which far exceeds the normal landing velocity (maximum aircraft velocity during reversing) of a short-haul aircraft.

Performance variation with exlet flare angle. - The variation in the data from all the flares tended to collapse to a much larger extent when compared at the same flare angle θ_e. The total pressure recovery P_1/P_0 for all solid-flare exlets is shown in figures 10(a) and (b) as a function of exlet flare angle θ_e for fan duct Mach numbers of approximately 0.34 and 0.46, respectively. In both parts of the figure, data are shown for free-stream Mach numbers of 0, 0.13, and 0.21 and for flare angles from 30° to 60°, with the 0°-flare exlet data included. The values of pressure recovery shown in figure 10(b) for the 0°-flare exlet are, however, extrapolated from the actual data, since a duct Mach number of 0.46 was not achieved at any time for that exlet. For $\theta_e = 30^\circ$, the solid lines connect the exlets having the same contraction ratio (CR = 2.11), and the dashed lines connect the exlets with the same flare length ($l_e/h = 0.89$).

Figure 10 illustrates that the data collapse well on the basis of flare angle. This result implies that the total pressure recovery (particularly when $M_0 = 0$) is largely controlled by the flare angle for the configurations of this report. In addition, the figure directly indicates the trend of total pressure recovery with flare angle and shows that the highest pressure recovery occurs for a flare angle of 30°. The curves of figure 10 between 0° and 30° (long-short dashed lines) are estimated trends since there are no

data in this range of large variation in total pressure recovery. In this range the curves are based qualitatively on the results of reference 7, which include data as low as $\theta_e = 20^o$.

Serrated-Flare Exlet

The results previously shown for the solid-flare exlets may suggest better aerodynamic performance than would actually be achieved by an exlet in an engine installation. A flared variable-geometry nozzle in all probability would not have the smooth, axisymmetric surfaces of a model exlet. For this reason, a serrated exlet with 15 notches (previously described with fig. 3(d)) was also tested. The geometry of the serrated exlet may be an extreme example; that is, the actual flared nozzle probably would not have as many (or as large) serrations. However, the results from the serrated exlet should yield an indication of the extent to which the aerodynamic performance of an axisymmetric exlet may be affected.

Figure 11 shows the total pressure recovery P_1/P_0 and the fan duct Mach number M_1 as a function of the free-stream Mach number M_0 for the serrated exlet and the smooth, axisymmetric exlet from which the serrated exlet was obtained. The data of figure 11 are presented in the same manner as those of figure 6. Figure 11(a) shows that the serrated exlet reduced the total pressure recovery by as much as 3 percent at the fan design speed (N/N_d = 100 percent). Figure 11(b) indicates a drop in the fan duct Mach number for the serrated exlet, which is associated with increased total pressure loss. It is expected that the total pressure loss due to the notches is proportional to the number of notches, and that a flare design with fewer (or smaller) notches would have a smaller loss.

Performance Details - Long 30^o-Flare Exlet

As stated previously in the section Solid-Flare Exlets, it was concluded that of the geometries investigated the highest total pressure recovery occurred for the long 30^o-flare exlet. Therefore, that exlet was selected for a more detailed study of its aerodynamic performance. The performance of the long 30^o-flare exlet is discussed in terms of total pressure recovery, fan duct Mach number, and fan duct total pressure distributions. The effects of free-stream Mach number and crossflow velocity are considered. Finally, a discussion is included on the possible effect of this exlet on the flow into a core inlet (fig. 1).

Effect of free-stream Mach number. - Figure 12 presents the total pressure recovery and the fan duct Mach number as functions of the free-stream Mach number. Data

are shown for fixed model fan speeds N/N_d of 40, 55, 70, 85, and 100 percent of design. Also shown on the figure is the ratio of free-stream static to total pressure.

The total pressure recovery of the long 30^o-flare exlet (fig. 12(a)) drops sharply as the free-stream Mach number is increased for all values of N/N_d. The exlet total pressure is always well below the free-stream static pressure. Also, as the N/N_d of the fan is increased (increased fan duct Mach number), there is a relatively small reduction in the exlet total pressure recovery.

The fan duct Mach number of the long 30^o-flare exlet (fig. 12(b)) also drops as the free-stream Mach number is increased for all values of N/N_d. This effect is the same as that discussed in the section on the performance of the unflared exlet. However, in the present case, the reduction in fan duct Mach number with free-stream Mach number is less severe. Also the regions of N/N_d and M_0 in which the free-stream flow backpressures the fan are less extensive for the flared exlet than for the unflared exlet.

Effect of crossflow. - Figure 13 presents the total pressure recovery P_1/P_0 and the fan duct Mach number M_1 for crossflow velocities V_c of zero and 20 meters per second. Data are shown as functions of the axial component of the free-stream Mach number M_a (defined by the inset sketch in fig. 13(a)) for the same fixed values of N/N_d as in the preceding figure. A comparison of the crossflow and no-crossflow cases shows that the crossflow component of the free-stream flow has reduced the total pressure recovery from 1 to 1.5 percent below the no-crossflow case. There is a similar reduction in the fan duct Mach number for the crossflow case, and the free-stream Mach number at which the fan/exlet model stalls (low rotational speeds) is lower for the crossflow case.

Fan duct total pressure distributions. - The discussion of the data in preceding sections is devoted to the consideration of average quantities indicative of the overall aerodynamic performance of the fan/exlet model. To adequately consider all aspects important to the operation of a fan in this type of flow, some consideration must be given to the detailed flow within the fan duct. Figure 14 illustrates the total pressure distribution at the rake measuring plane for the long, 30^o-flare exlet. The distributions are shown for a fan duct Mach number of approximately 0.46 over a range of free-stream Mach number from zero to 0.21 and for cases without and with a crossflow velocity. In all cases, the view is taken in the direction of the fan flow (or viewing upstream with respect to the free-stream flow).

Figures 14(a) to (d) present the fan duct total pressure distributions over a range of free-stream Mach number without any crossflow component. The most notable feature of these pressure distributions is that the lines of constant total pressure recovery are nearly concentric rings about the model axis. As the free-stream velocity increases, the lines of constant total pressure recovery remain concentric rings but extend farther from the outer wall toward the model centerbody. Obviously, for the case of no crossflow the variation in total pressure is virtually limited to a radial variation.

Figure 14(e) shows the total pressure distribution for a pure crossflow velocity of 20 meters per second ($M_a = 0$). In this case, there is an obvious depression in the total pressure distribution on the crossflow side of the nacelle. Figure 14(f) presents the results for a combined free-stream Mach number of 0.11 and a crossflow velocity of 20 meters per second. This last figure appears as a combination of the distributions of figures 14(c) and (e). For all cases that include a crossflow component, the total pressure distributions include both radial and circumferential variations.

Fan duct total pressure distortion. - Considering the unusual nature of the flow patterns associated with the fan/exlet system during reversing, the levels of fan duct flow distortion which feed into the fan are important. This fan duct flow distortion upstream of the fan may increase fan noise or fan blade vibrational stress in the same fashion as an inlet flow distortion would for the case of forward-thrust operation. Figure 15 presents a fan duct total pressure distortion parameter D for the internal flow as a function of the axial component of the free-stream Mach number M_a. The parameter D is the difference between the maximum and minimum total pressure measurements at the rake measuring plane ratioed to the area-averaged total pressure P_1. Data are shown in figure 15 for fixed N/N_d of 40, 55, 70, 85, and 100 percent.

Figure 15(a) presents the flow distortion data for the no-crossflow ($V_c = 0$) case; figure 15(b) contains the data for the crossflow case of $V_c = 20$ meters per second. In both parts of the figure, the value of the distortion parameter is shown to be dependent on both the free-stream Mach number and the fan percentage of design speed. The maximum values of D are 0.10 and 0.17 for the no-crossflow and crossflow cases, respectively. The distortion parameter D would have a larger magnitude than any other commonly used method of calculating a distortion index (referenced to the average total pressure P_1), and the levels of the distortion are not high. Therefore, it has been assumed for the work of this report that fan flow distortion in this situation is of secondary importance. This result is unexpected, since the previously shown values of total pressure recovery can be low. However, the low pressure recovery and low distortion flow result because the reduced pressure recovery occurs over a large extent of the entire passage rather than being concentrated in a small region within the passage.

This distortion parameter is determined at the rake measuring plane and not at the fan face (the usual distortion reference station). Hence, the results of figure 15 cannot be used to predict the fan face distortion, especially if there are additional disturbances (stators, struts, or flow splitters) present in the actual fan duct. Finally, since there is no information available on the distortion levels that a reversed-pitch fan will accept, the question of the acceptability of the level or type of flow distortion cannot even be discussed until there is a further definition of the fan characteristics.

Effect of exlet performance on core inlet flow. - The total pressure of the core inlet flow in a fan/jet engine is of importance since the core engine provides the power to operate the fan and is particularly sensitive to any losses in the flow. If the core inlet

flow is drawn from the rear portion of the engine (as shown in fig. 1), the flow must incur whatever losses are associated with the exlet prior to intake to the core. However, the core inlet flow is taken from that portion of the fan duct flow that is closest to the centerbody. This means that, in order to consider any possible effect of the exlet performance on the core inlet flow, the flow characteristics of the fan duct flow in the vicinity of the centerbody must be known. These characteristics are determined in this section even though the core flow itself was not simulated during the test program. It has been assumed that the absence of the core flow has little or no effect at the measuring station, though its absence would be significant in other regions of the model.

Figure 16 presents the total pressure recovery for the inner and outer passages of the fan duct at the rake measuring plane for the long, 30^{o}-flare exlet. The inner-passage and outer-passage pressure recovery values are calculated in the same manner as the overall pressure recovery except that the innermost three tubes on each rake and then the outermost three tubes on each rake are used respectively. Figure 16 presents the data in the same manner as figure 12(a), the overall pressure recovery for this exlet.

Figure 16(b) shows that the inner-passage pressure recovery (region of interest to the core inlet flow) acts differently than either the complete passage pressure recovery (fig. 12(a)) or the outer-passage pressure recovery (fig. 16(a)). Up to a free-stream Mach number of 0.13, there is little variation in the inner-passage pressure recovery with percentage of design speed (or fan duct Mach number). However, for $M_0 \geq 0.13$, the lowest fan percentage of design speed yields the lowest inner-passage pressure recovery. This means that as the percentage of design speed (or fan duct Mach number) is increased the losses in total pressure are increasingly localized to the outer portion of the fan duct (fig. 14).

The inner-passage total pressure recoveries (fig. 16(b)) are higher than the overall passage pressure recoveries (fig. 12). For 100 percent of design speed (or high fan duct Mach number), the total pressure loss in the inner passage is always less than one-third of the loss in the outer passage. However, the pressure recoveries of the inner and outer passages for 40 percent of design speed are within 1 percent, with the inner passage having a slightly higher recovery. The core would draw flow from the region of the fan duct flow having the highest pressure recovery. The actual value of that pressure recovery, of course, depends on the quantity of mass flow taken into the core.

The data in figure 17 indicate the maximum value that may be assumed for the core-inlet-flow total pressure prior to intake in the core. Shown in this figure is the innermost-ring average total pressure ratioed to the free-stream static pressure (for convenience) as a function of free-stream Mach number. Data are shown for all values of the percentage of design speed N/N_d. The innermost-ring total pressure is the arithmetic average of the total pressure measurements of the eight tubes closest to the model centerbody. Since the maximum total pressure always occurs in the region

closest to the centerbody (fig. 14), the data of figure 17 indicate that the maximum value of the total pressure in the fan duct could be closely approximated by the free-stream static pressure. This is particularly true at low free-stream Mach numbers. In summary, a combination of the results of figures 16 and 17 indicate that the total pressure of the flow drawn into the core is higher than the average fan duct total pressure but has an approximate maximum value equal to the free-stream static pressure.

Exlet Surface Pressures

Static pressure measurements were made along both the internal and external flare surfaces to obtain the pressure differential across the flare, which determines the load on the flared exlet. There is also a need for the surface static pressure measurements if the analysis of reference 6 is to be extended to flared exlets. In addition, some data were also obtained from the external total pressure instrumentation (also previously described) which were intended only to yield the direction of the flow (i. e., whether it was in the direction of the free-stream flow or opposite to that direction). There was no previous information available related to the flow direction along the external flare surface, and that information would be beneficial in determining a model and analysis of flow in the region of the exlet.

Shown in figure 18 are the internal and external surface static pressure measurements for the nominal 45°-flare exlet ratioed to the free-stream total pressure as a function of distance along the flare surface. The point of junction between the flare and the fan duct (point A) and the exlet tip (point B) are noted on the abscissa. Data are presented for six values of the free-stream Mach number M_0 but are restricted to a fan duct Mach number M_1 of 0.46 and no crossflow velocity ($V_c = 0$). The multiple symbols at a given station represent the data at various circumferential locations on the exlet (see section Fan/Nacelle Model).

The maximum pressure differential across the flare is shown in figure 18 to be approximately 20 percent of the free-stream total pressure. This high value occurs close to the exlet tip at the highest free-stream Mach number of 0.21. As the free-stream Mach number is reduced, the pressure differential is reduced to a value of 10 percent of the free-stream pressure at $M_0 = 0$. The low surface static pressures near the exlet tip plus the higher-valued static pressures in the middle of the internal exlet surface may indicate that a ring vortex is formed in the vicinity of the exlet tip with a stagnation point located between points A and B of the internal exlet surface.

Measurements of the total pressure immediately above the external flare surface are not reported quantitatively in this report since these measurements were made only to determine qualitatively the direction of the flow along the external flare surface. These measurements indicate that the flow along the external flare surface is in the di-

rection of the exlet tip (flow toward point B, fig. 3). The only exception to the preceding statement occurred for the case of a pure crossflow (V_c = 20 m/sec, M_a = 0). In that case, the total pressure measurements on the leeward side of the exlet are approximately equal, as expected.

SUMMARY OF RESULTS

An experimental investigation was conducted to determine the aerodynamic performance of nine flared fan nozzles (exlets) when used as inlets for reverse flow in a simulated turbofan-engine fan exhaust duct. The tests were performed by inverting the intake and discharge of a model fan with respect to a free-stream flow so that the fan flow entered the fan after passing through the downstream-facing flared fan nozzle (exlet). This was done to simulate the flow fields associated with a variable-pitch fan during thrust reversal. The primary results of this investigation may be summarized as follows:

1. The best criterion for the aerodynamic performance of an exlet is the fan duct total pressure recovery. Fan flow distortion levels are assumed to be low until further definition of the problem. The effect of the free-stream flow backpressuring the fan is dependent on the exlet pressure recovery and fan total pressure rise (or percentage of fan design speed).

2. The widest variation in exlet pressure recovery due to variations in exlet geometry occurs at the free-stream static condition (M_0 = 0). With a free-stream Mach number (different than zero), the pressure recovery measurements of the various exlets are similar in value if the contraction ratio CR (exlet tip area ratioed by the fan duct area) is sufficiently high (e.g., for these tests, CR $\geq$ 1.74).

3. Increasing the free-stream Mach number significantly reduces the pressure recovery of all exlets and reduces the differences among the exlets.

4. Of the exlets tested, the exlet having the best aerodynamic performance has a flare angle θ_e of 30° and a contraction ratio CR of 2.11.

5. For the exlet having the best performance, a crossflow velocity (free-stream flow perpendicular to the model centerline) of 20 meters per second reduces the no-crossflow pressure recovery by approximately 1 percent and increases the maximum value of the total pressure distortion parameter (maximum minus minimum pressure divided by the average pressure) from 0.10 to 0.17.

6. The aerodynamic performance (in terms of total pressure recovery and fan duct mass flow) is poor for the 0°-flare exlet (the unflared exlet or representative forward-thrust nozzle).

7. An exlet with serrated (petal) surfaces can reduce the total pressure recovery of the fan flow by as much as 3 percent when compared to an axisymmetric exlet.

Lewis Research Center,
National Aeronautics and Space Administration,
Cleveland, Ohio, November 14, 1975,
505-05.

REFERENCES

1. Denning, R. M.: Variable Pitch Ducted Fans for STOL Transport Aircraft. ASME Paper 72-GT-61, Mar. 1972.
2. Davis, D. G. M.: Variable Pitch Fans - Progress in Britain. Flight Intern., vol. 103, April 1973, pp. 615-617.
3. Wilson, Michael: Variable Pitch Fans - Hamilton Standard and the Q-Fan. Flight Intern., vol. 103, April 1973, pp. 617-619.
4. Wesoky, H. L.; and Steffen, F. W.: Wind Tunnel Tests of a 20 Inch Diameter 1.15 Pressure Ratio Fan Engine Model. AIAA Paper 73-1216, Nov. 1973.
5. Wesoky, Howard L.; et al.: Low-Speed Wind Tunnel Tests of a 50.8-Centimeter (20-In.) 1.15-Pressure-Ratio Fan Engine Model. NASA TM X-3062, 1974.
6. Keith, Theo G., Jr.: Subsonic Flow into a Downstream Facing Inlet. J. Aircraft, vol. 11, no. 4, April 1974, pp. 251-252.
7. Vier, W. F.: Quiet, Clean, Short-Haul Experimental Engine (QCSEE) Test Results from a 14 cm Inlet for a Variable Pitch Fan Thrust Reverser. (General Electric Co.; NAS3-18021) NASA CR-134867, 1975.
8. Performance of a 5.5-Inch Diameter Axial Fan with Various Inlets and Exits. Rep. 708-1, Tech Development, Inc., 1970.
9. Miller, Brent A.; and Abbott, John M.: Aerodynamic and Acoustic Performance of Two Choked Flow Inlets under Static Conditions. NASA TM X-2629, 1972.
10. Yuska, Joseph A.; Diedrich, James H.; and Clough, Nestor: Lewis 9- by 15-Foot V/STOL Wind Tunnel. NASA TM X-2305, 1971.

TABLE I. - CONFIGURATIONS TESTED AND THEIR PRESSURE RECOVERIES

Configuration	Description	Symbol	Schematic	Flare angle, θ, deg	Flare contraction ratio, CR	Flare length ratio, l_e/h	Total pressure recovery, ($M_0 = 0$, $M_1 = 0.46$), P_1/P_0
1	Nominal, 45^o flare	○	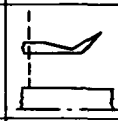	45	2.11	0.89	0.987
2	Short, 30^o flare	□	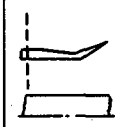	30	1.74	0.89	0.992
3	Short, 60^o flare	◇	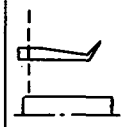	60	2.11	0.73	0.972
4	Long, 30^o flare	△	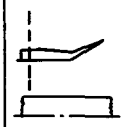	30	2.11	1.26	0.996
5	Short, 45^o flare	◺	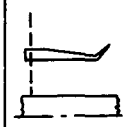	45	1.51	0.45	0.989
6	Long, 45^o flare	◺	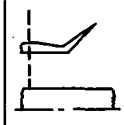	45	2.74	1.30	0.981
7	Long, 60^o flare	⌂		60	2.41	0.89	0.969
8	0^o flare or forward-thrust exit	◇	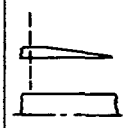	0	1.00	----	[a]0.86
9	Serrated, 45^o flare	⌂	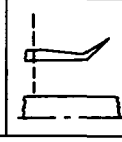	45	2.11	0.89	0.969

[a]Estimated.

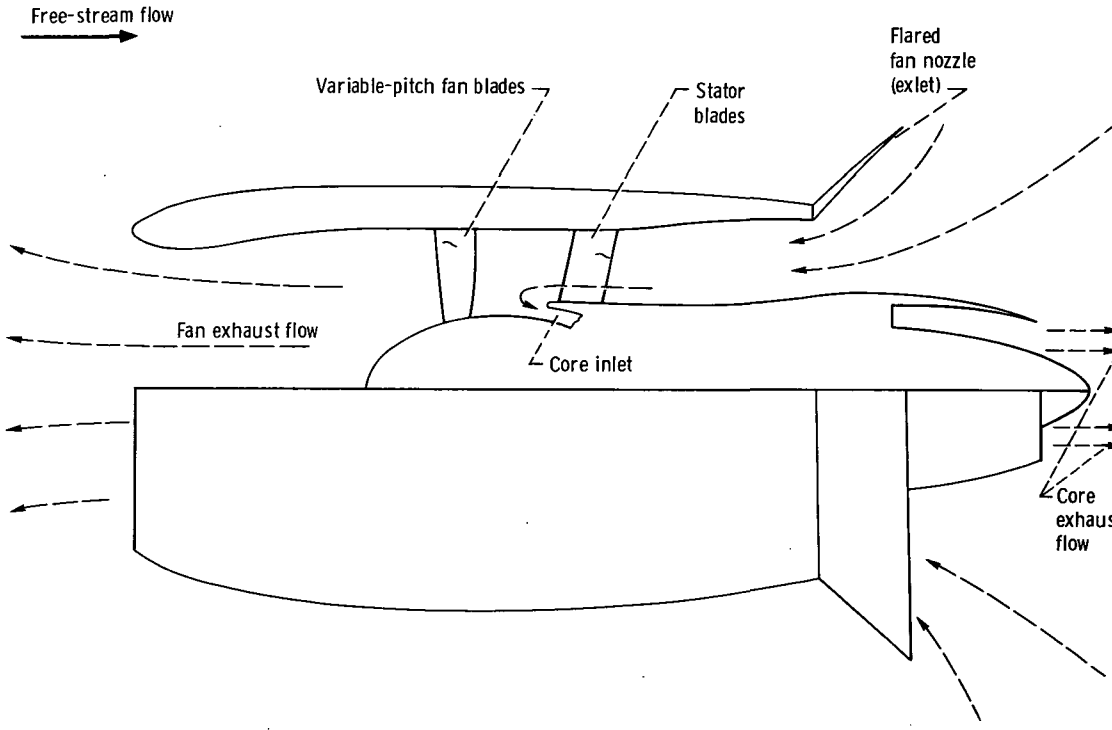

Figure 1. - Elements of a variable-pitch fan engine during reverse-thrust operation.

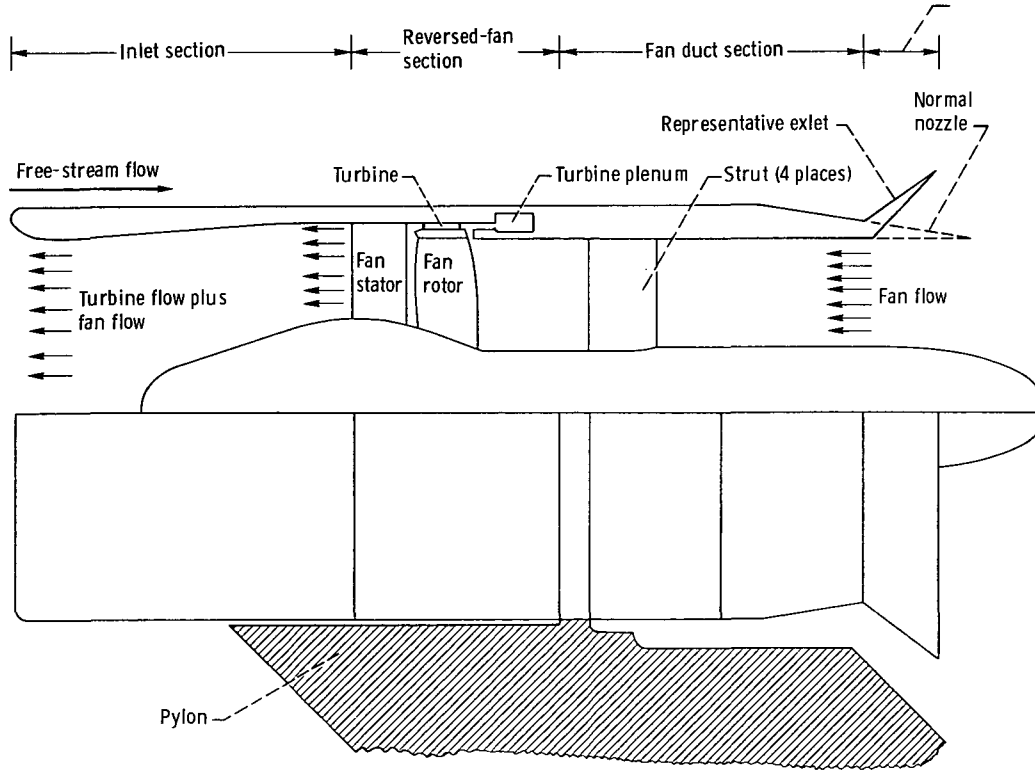

Figure 2. - Fan nacelle model with exlet.

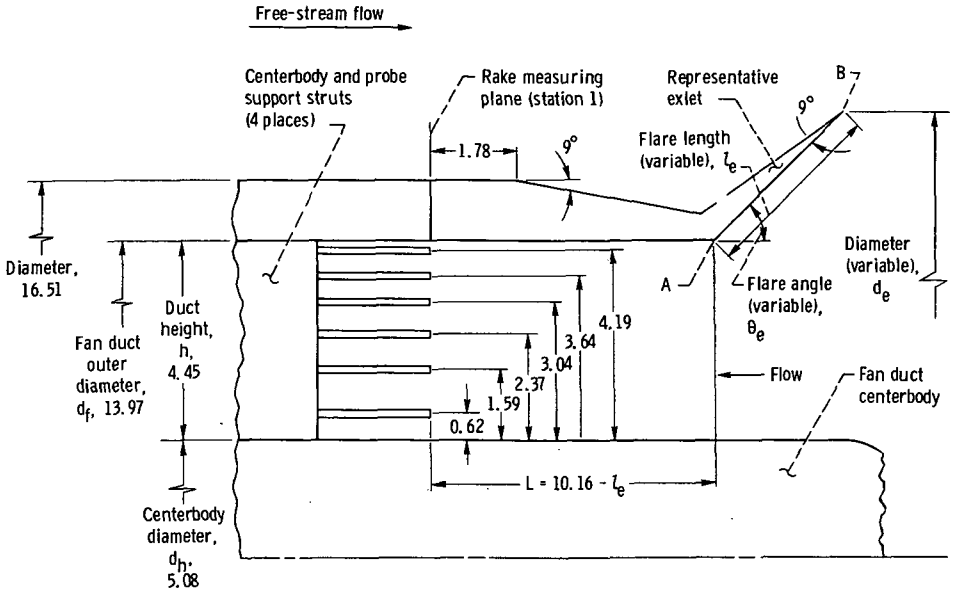

(a) Cross section of model.

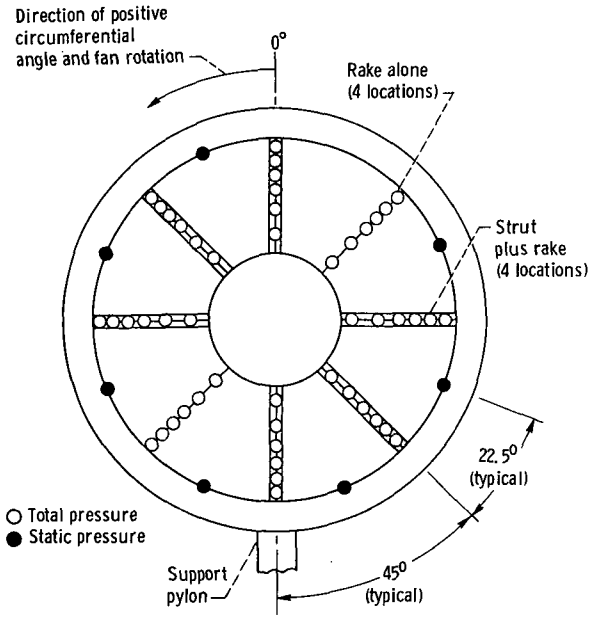

(b) Transverse section through model at rake measuring plane (view downstream with respect to fan flow).

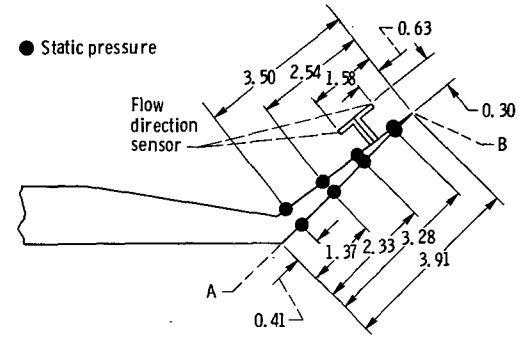

(c) Exlet instrumentation.

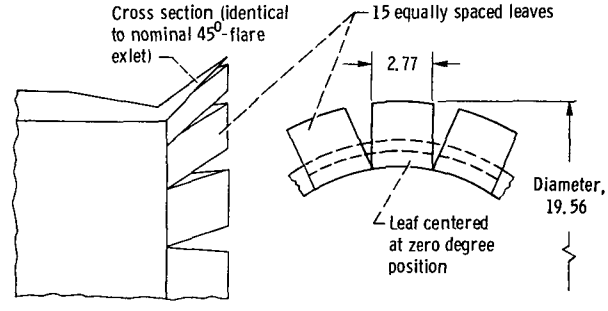

(d) Serrated-flare exlet geometry.

Figure 3. - Exlet geometry and instrumentation. Dimensions are in centimeters.

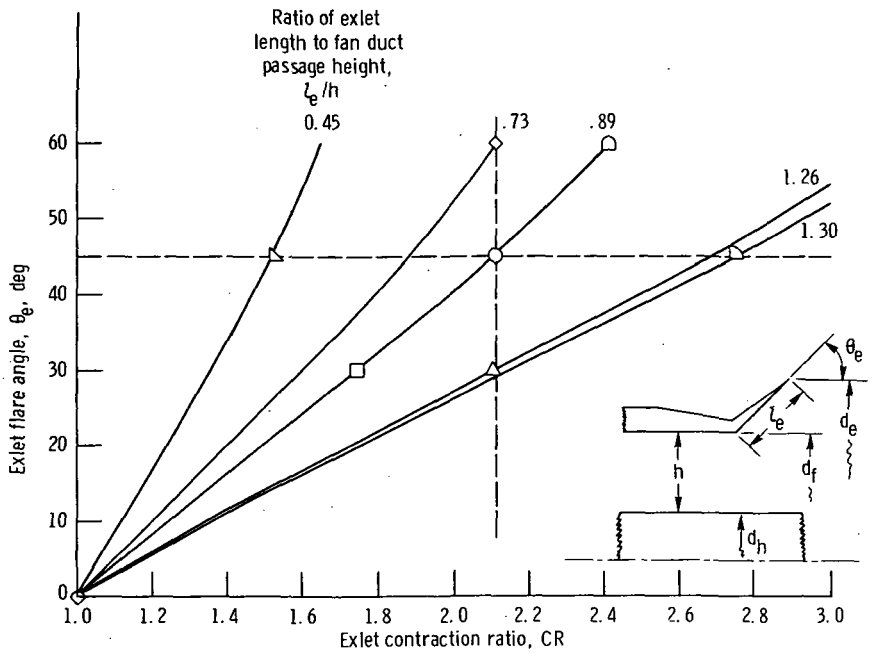

Figure 4. - Exlet test configuration matrix.

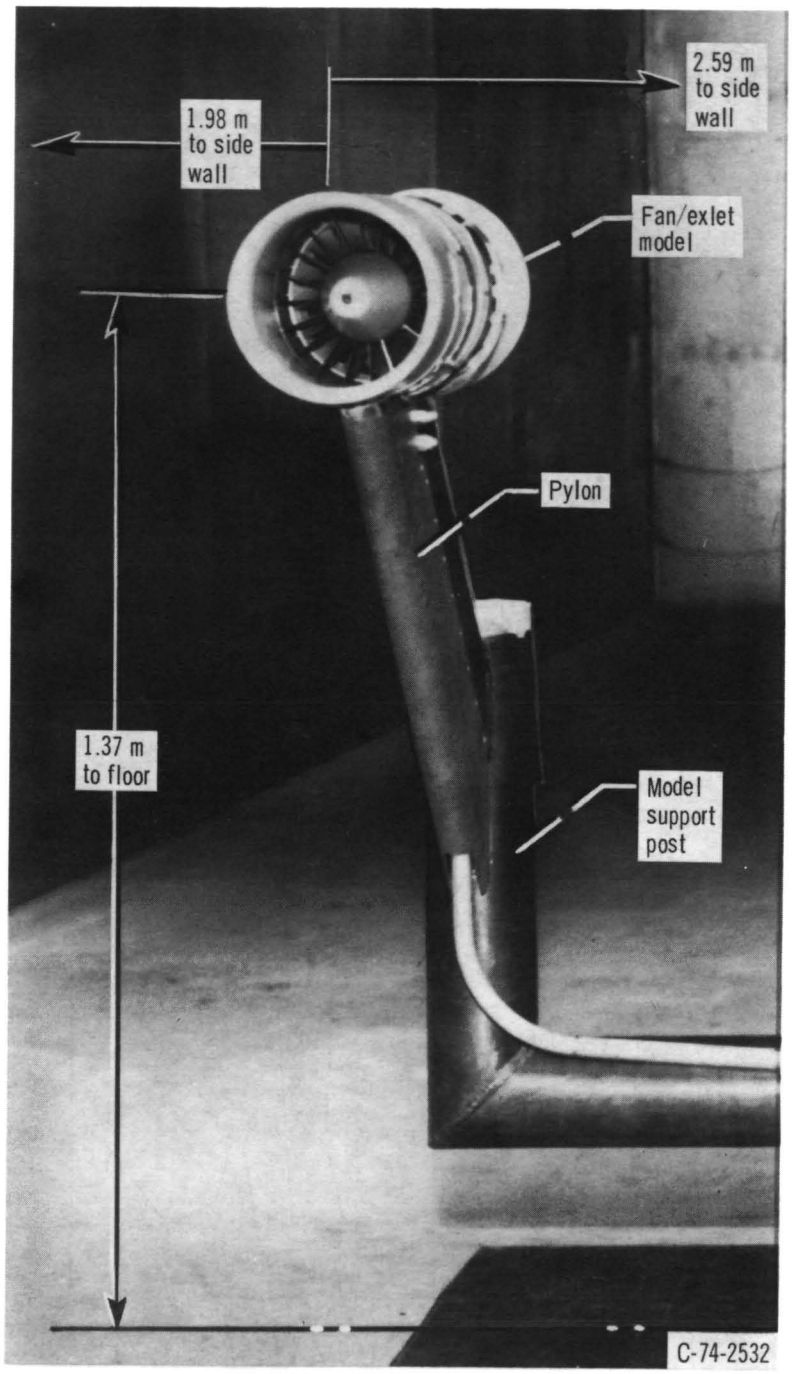

Figure 5. - Fan/exlet model located in low-speed wind tunnel (view downstream with respect to free-stream flow).

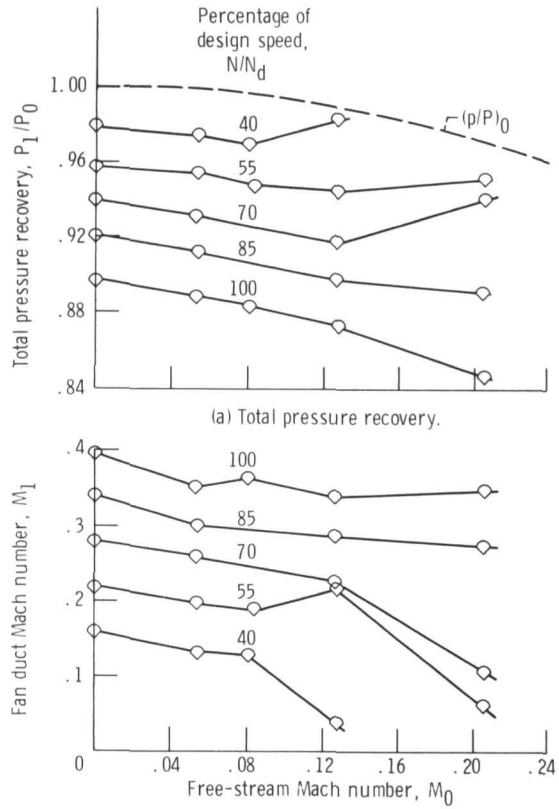

(b) Fan duct Mach number.

Figure 6. - Variation of total pressure recovery and fan duct Mach number for 0°-flare exlet with zero crossflow velocity (V_c = 0).

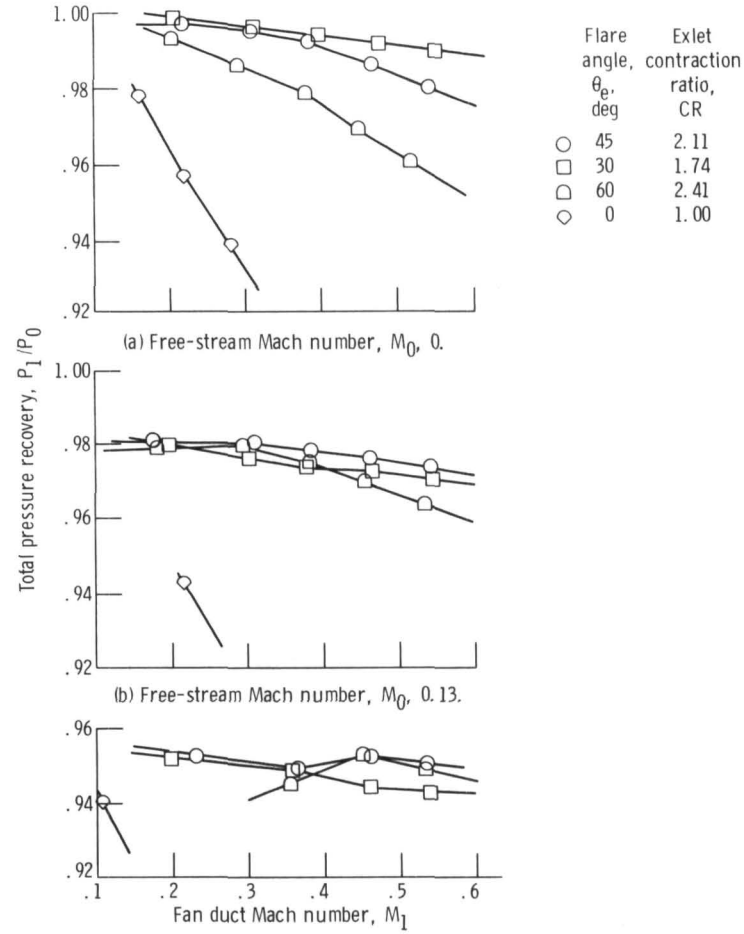

Figure 7. - Variation of exlet total pressure recovery with fan duct Mach number for all solid-flare exlets having the same flare length (l_e/h = 0.89). Zero crossflow velocity (V_c = 0).

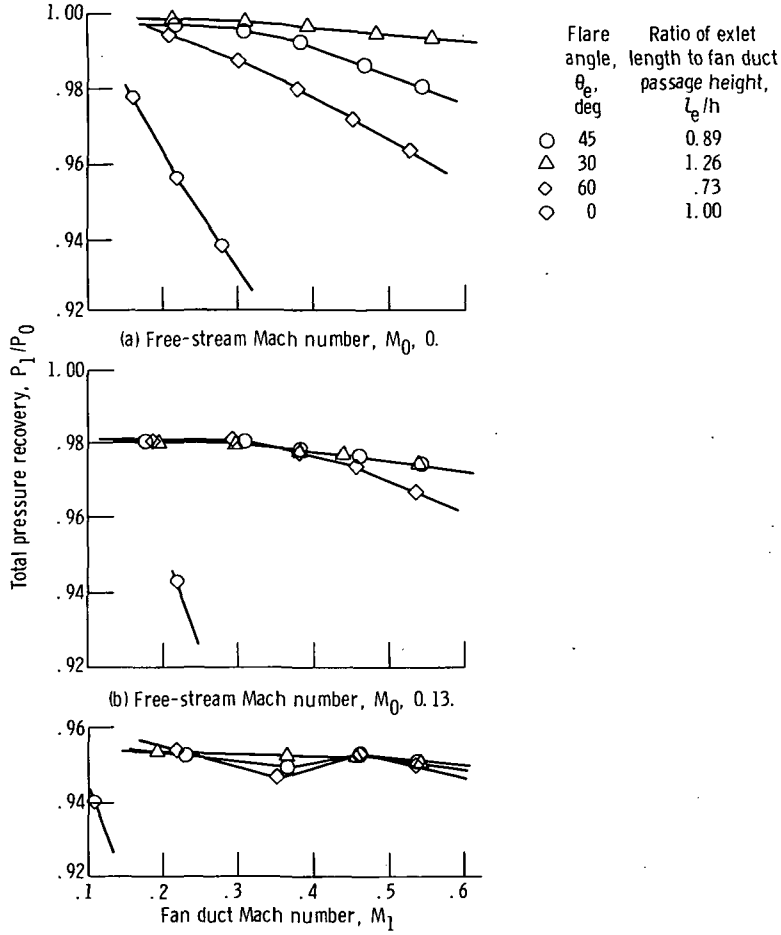

Figure 8. - Variation of exlet total pressure recovery with fan duct Mach number for all solid-flare exlets having same contraction ratio (CR = 2.11). Zero crossflow velocity (V_c = 0).

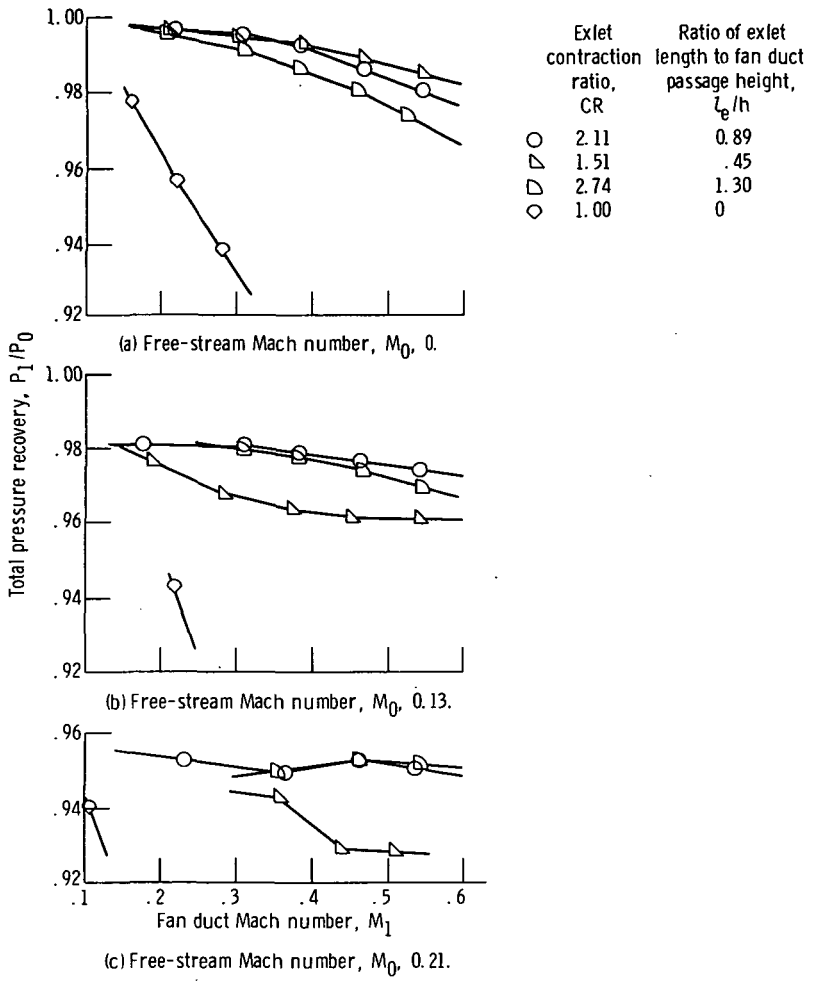

Figure 9. - Variation of exlet total pressure recovery with fan duct Mach number for all solid-flare exlets having same flare angle ($\theta_e = 45^0$). Zero crossflow velocity ($V_c = 0$).

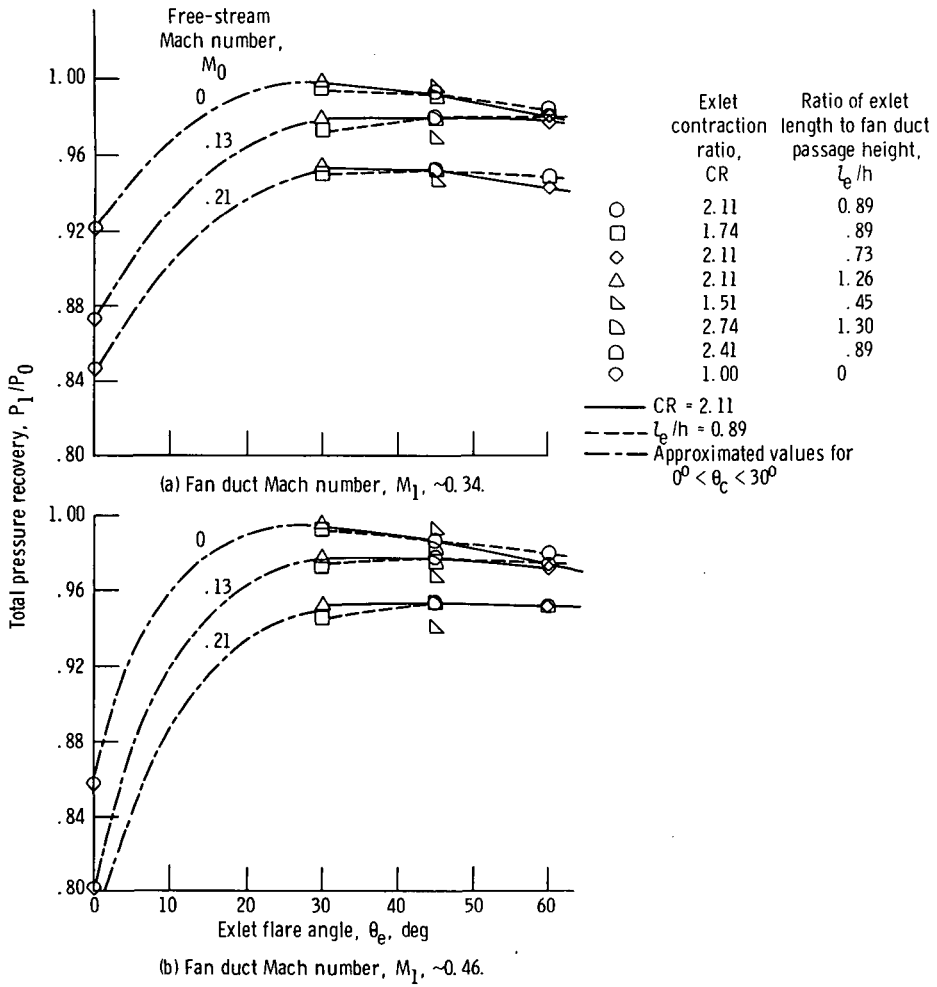

(a) Fan duct Mach number, M_1, ~0.34.

(b) Fan duct Mach number, M_1, ~0.46.

Figure 10. - Variation of exlet total pressure recovery with flare angle for all solid-flare configurations. Zero crossflow velocity (V_c = 0).

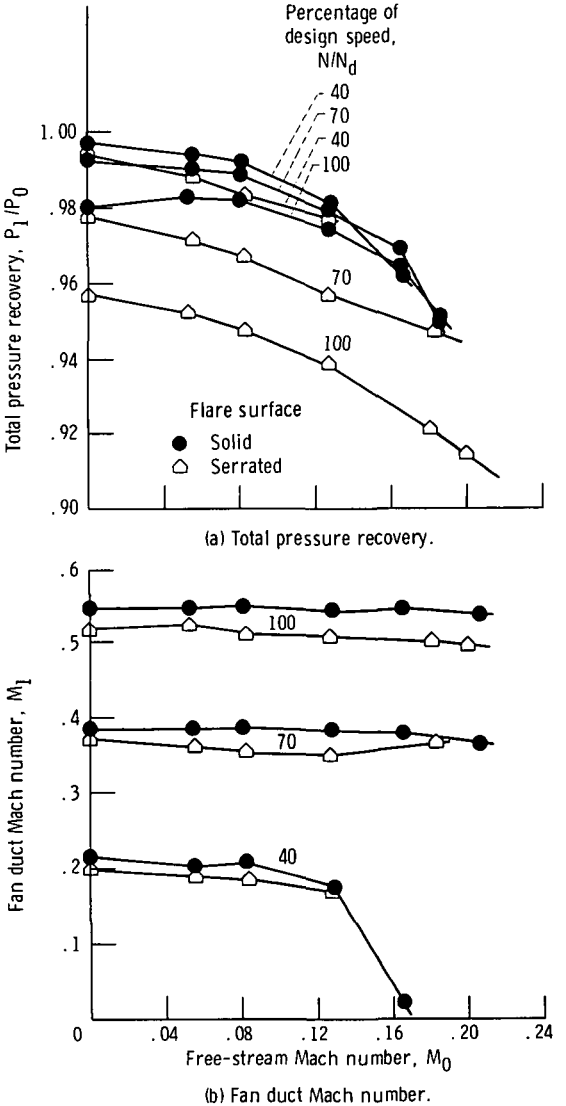

(a) Total pressure recovery.

(b) Fan duct Mach number.

Figure 11. - Effect of flare serration on total pressure recovery and fan duct Mach number. Zero crossflow velocity (V_c = 0).

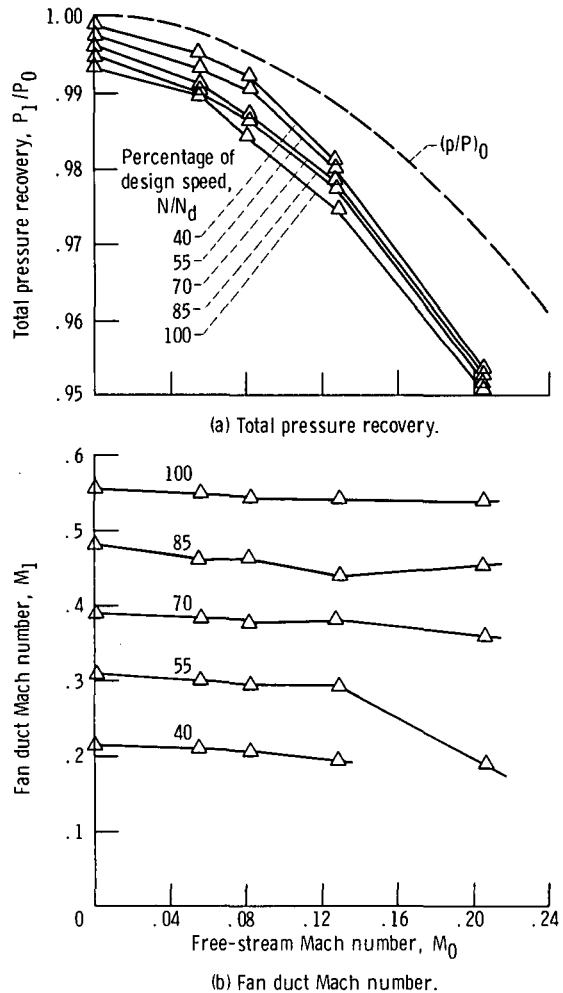

Figure 12. - Variation of total pressure recovery and fan duct Mach number with free-stream Mach number for long, 30°-flare exlet. Zero crossflow velocity (V_c = 0).

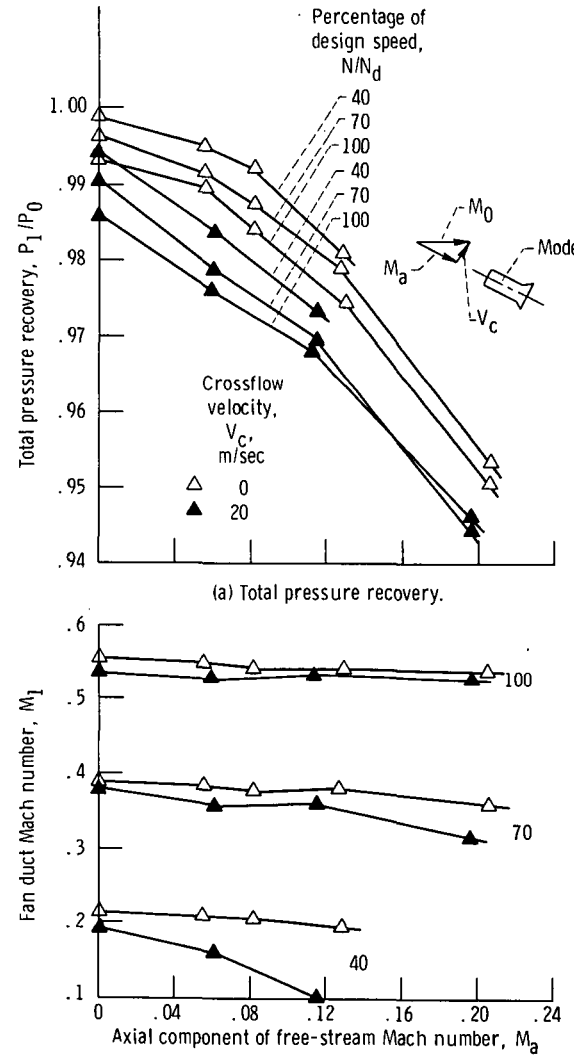

Figure 13. - Variation of total pressure recovery and fan duct Mach number with crossflow for long, 30°-flare exlet.

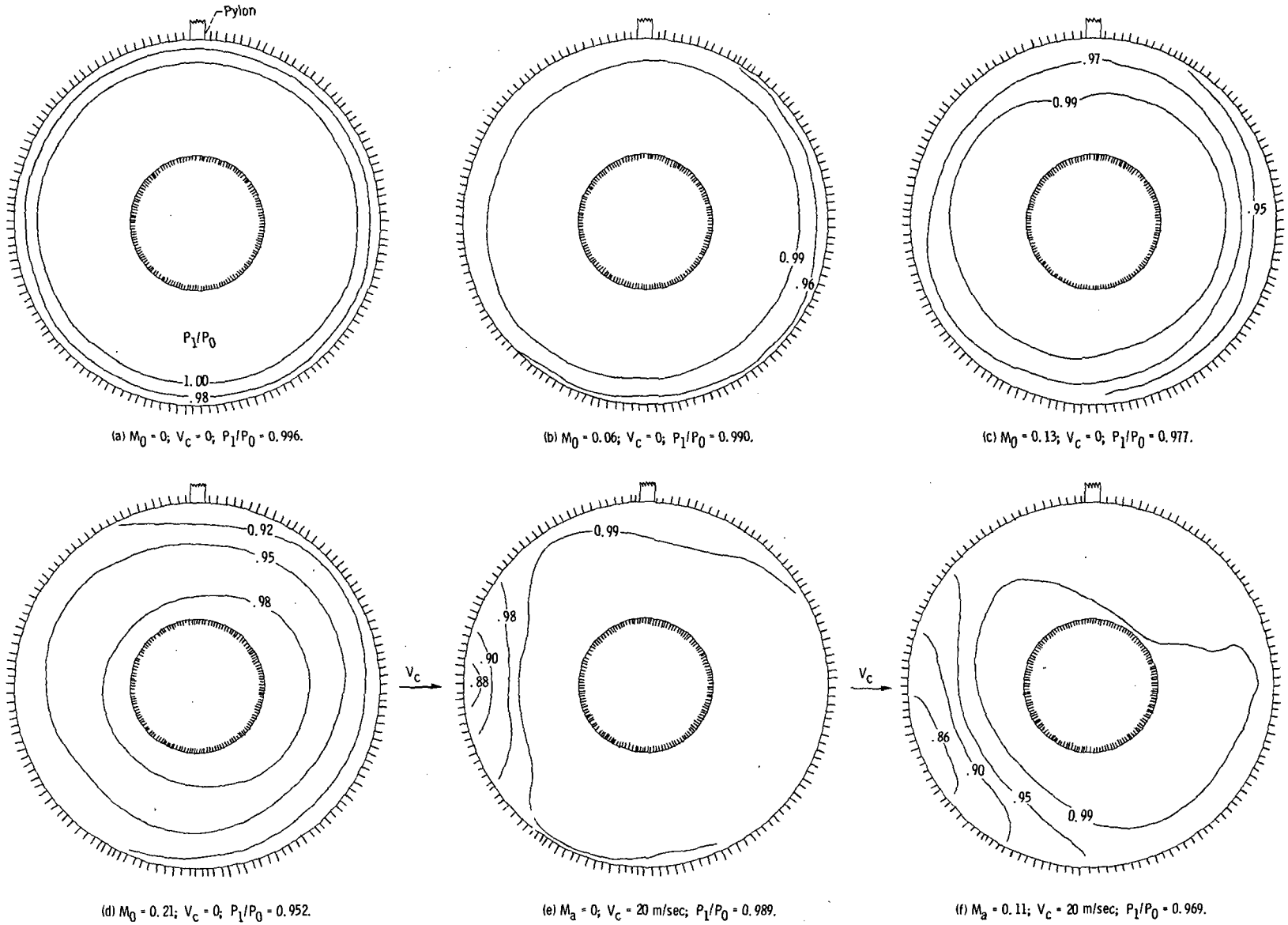

(a) $M_0 = 0$; $V_c = 0$; $P_1/P_0 = 0.996$.

(b) $M_0 = 0.06$; $V_c = 0$; $P_1/P_0 = 0.990$.

(c) $M_0 = 0.13$; $V_c = 0$; $P_1/P_0 = 0.977$.

(d) $M_0 = 0.21$; $V_c = 0$; $P_1/P_0 = 0.952$.

(e) $M_a = 0$; $V_c = 20$ m/sec; $P_1/P_0 = 0.989$.

(f) $M_a = 0.11$; $V_c = 20$ m/sec; $P_1/P_0 = 0.969$.

Figure 14. - Example total pressure distributions for long, 30°-flare exlet at various free-stream Mach numbers M_0, crossflows V_c, and total pressure recoveries P_1/P_0. Fan duct Mach number, M_1, ~0.46.

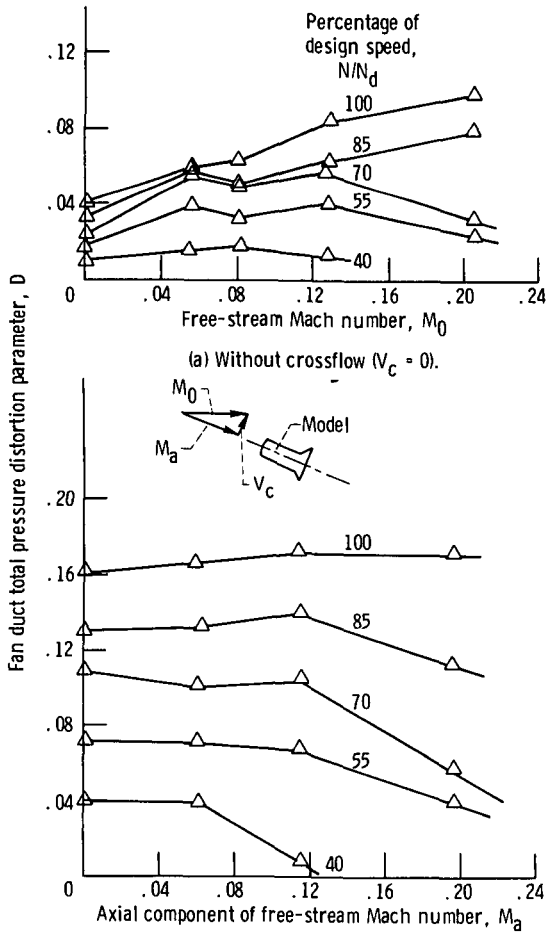

Figure 15. - Variation of fan duct total pressure distortion parameter with free-stream Mach number for long, 30°-flare exlet.

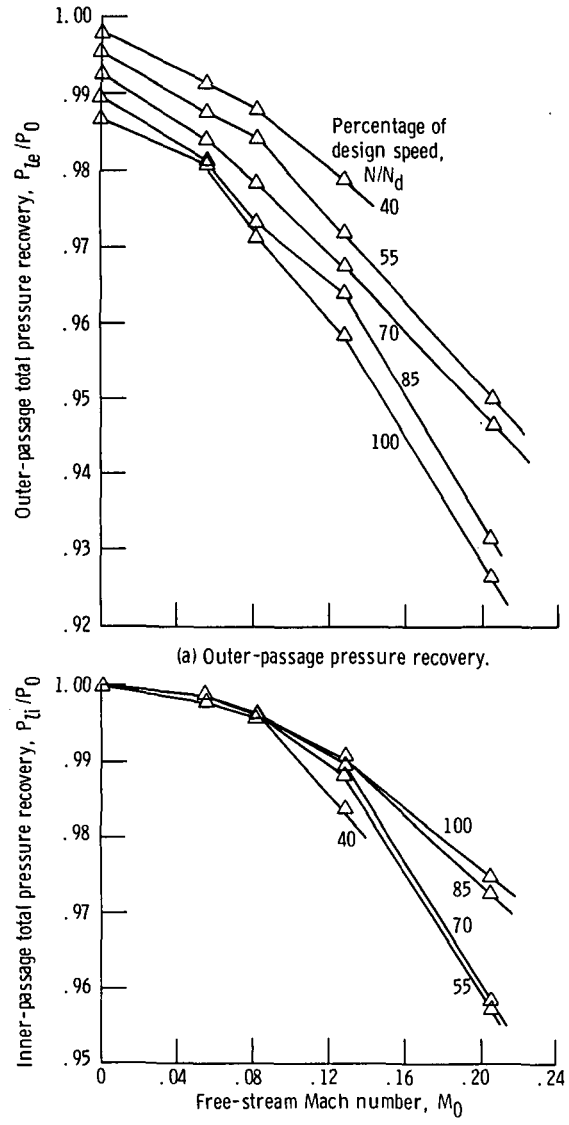

Figure 16. - Variation of inner- and outer-passage total pressure recovery with free-stream Mach number. Zero crossflow velocity (V_c = 0).

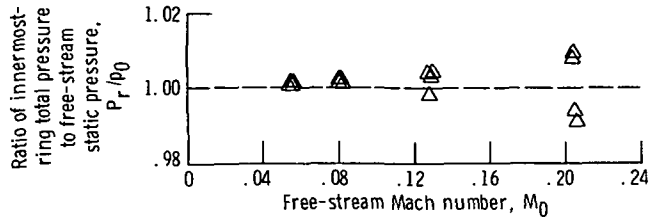

Figure 17. - Variation of innermost-ring total pressure ratioed to free-stream static pressure with free-stream Mach number. Zero crossflow velocity (V_c = 0).

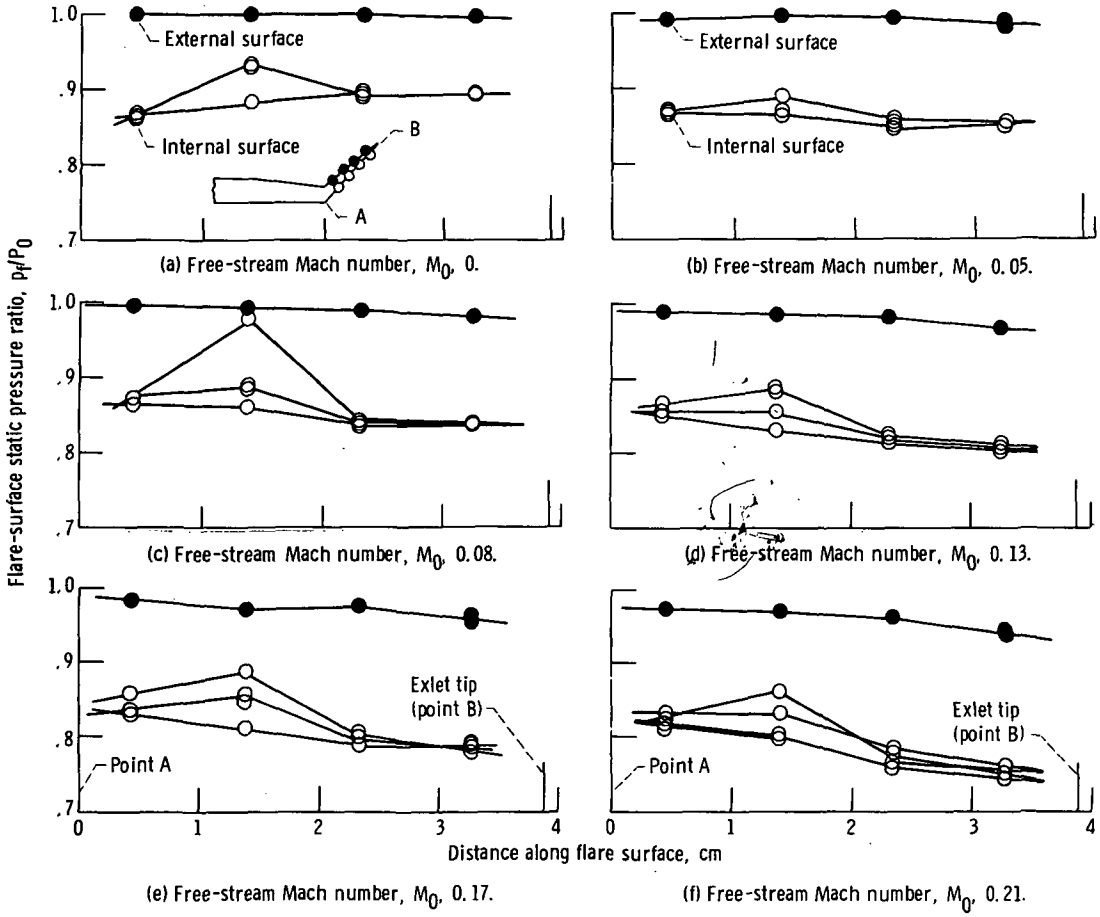

Figure 18. - Variation of flare-surface static pressure with distance along surface for nominal 45°-flare exlet. Zero crossflow velocity (V_c = 0); fan duct Mach number, M_1, ~0.46.